

To be published in Journal of the Optical Society of America B:

Title: Theoretical Optimization of Transverse Waveguiding in Oxide-Confined VCSELs with Internal Photonic Crystals

Authors: Pavel Ivanov and Judy Rorison

Accepted: 1 November 2009

Posted: 3 November 2009

Doc. ID: 112961



Theoretical Optimization of Transverse Waveguiding in Oxide-Confined VCSELs with Internal Photonic Crystals

Pavel Ivanov* and Judy Rorison

*Electrical and Electronic Engineering Department, University of Bristol, Queen's Building,
University Walk, Bristol, BS8 1UB, United Kingdom*

**Corresponding author: p.ivanov@bristol.ac.uk*

Abstract: We systematically investigate transverse optical modes in oxide-confined vertical cavity surface emitting lasers (VCSELs) with photonic crystal (PC) structures embedded within the cavity of the VCSEL. We consider the interplay between the effective refractive index step of the oxide and the semiconductor and the oxide aperture size. The PC lattice period a , the diameter of the holes d and the number of lattice periods around the central defect are considered. We evaluate confinement factors for the various transverse modes and consider their spatial extent in the transverse plane which we relate to the out-put power. Results suggest that the power of the single-mode PC-VCSELs is limited by the smaller radius of the fundamental mode of the PC-VCSEL compared to the VCSEL with no PC. We discuss various designs aimed to optimize power into the single fundamental mode and to discriminate from power going into other modes.

2009 Optical Society of America

OCIS codes: 140.3430, 140.4780.

Introduction

Semiconductor Vertical-Cavity Surface-Emitting Lasers (VCSELs) are short-cavity single-longitudinal mode low threshold and low-cost lasers used in short-distance fibre-optical telecommunication networks. They consist of an active region contained in a high reflectivity cavity region defined by distributed Bragg reflectors (DBRs) on the top and bottom of the cavity. They allow low injection current, allow high modulation speed and produce a circular beam shape [1]. Although the longitudinal cavity of a VCSEL, as defined by the DBRs, is short reducing inter-longitudinal mode competition, the cavity is wide in the transverse plane supporting multiple transverse modes resulting in inter-transverse mode competition. This inter-transverse mode competition results in the output beam changing from its circular shape which is a major drawback. In addition, the use of single-transverse-mode VCSELs in fibre-optical networks reduces the modal dispersion, laser-to-fiber connection loss and noise. To establish single-transverse mode radiation output from VCSELs, small apertures are defined for the current injection by oxidation or proton-implanting. A small radius of the VCSEL aperture results in low radiation output due to a reduced active area and also introduces thermal problems.

A novel VCSEL was recently introduced by the incorporation of a two-dimensional photonic crystal (PC) waveguide within the VCSEL to control the transverse optical modes and establish single-mode radiation [2-5]. Thus transverse optical modes in this PC-VCSEL were to be controlled by the PC similarly to PC-fibres [6]. One or more holes in the centre of the VCSEL were omitted in order to form a defect in the PC and allow single-mode guiding. Experimentally PC-VCSELs, in which holes were made in the top distributed Bragg reflectors (DBRs), have demonstrated single-mode radiation but at significantly reduced output compared to the non-PC-VCSEL with multi-mode output. These PC-VCSELs have the PC holes etched

through the top set of DBRs using focussed ion beam or e-beam etching and/or reactive ion etching.

The origin of this power loss is not fully understood because the understanding of PC-VCSEL physics and its optimisation are not sufficient. Models of PC-VCSELs have been developed in which the holes are contained within the VCSEL cavity or through the entire VCSEL [4,7]. Relatively simple optical models of PC-VCSELs relying on the numerical solution of the partial differential Helmholtz and Maxwell equations provide information about the optical modes confined within the PC defect [4,5,7]. Recently the importance of the location of the holes (through the entire structure, cavity or DBRs) and the resulting losses incurred by various modes has started to be understood [8-10]. The understanding of such structures and the interplay between losses and PC effects is an area of on-going study. Dynamic models of PC-VCSELs [11,12] rely on numerical solutions of rate equations of the carriers and the PC-VCSEL optical models. This modeling can become very slow if approximations to the optical models cannot be made.

It is unclear whether the power loss in PC-VCSELs is due to the fabrication of the holes into the top DBR which reduces its reflectivity and introduces losses, whether it is related to the area of the VCSEL active region which is linked to the radial spatial extent of the transverse optical mode or whether it is related to spatial hole-burning. It may be that the PC patterns used are not properly optimized. In this paper we investigate transverse wave-guiding in oxide-confined PC-VCSELs with holes made only in the cavity. This type of structure involving growth interrupts is being investigated [13] and similar types of structures have been demonstrated by others [14]. It is believed that this model is also appropriate for holes etched through the entire VCSEL structure if the mode intensity is negligible in the PC holes as then

there will be no losses in the holes in the DBR. Optimal geometrical parameters of the PC and the oxide radius are established using a reasonable simple waveguide model that has been chosen because it can be easily used for dynamic modeling of PC-VCSELs [11]. Detailed optical models of PC-VCSELs such as [8,15] cannot be used because of their complexity.

The paper is organized as follows. Firstly, the modeled VCSEL structure and the waveguide model will be described. Secondly, the single-mode conditions of the PC fibre waveguides will be considered. Thirdly, effects of the PC waveguide on the single-mode conditions and the power in the fundamental mode of the oxide-confined PC-VCSELs will be investigated. Fourthly, the optimal size of the PC waveguide will be addressed.

Description of the investigated PC-VCSEL and the waveguide model

Oxide-confined GaAs/AlGaAs VCSELs emitting at 850 nm wavelength (in vacuum) are investigated. The epitaxial VCSEL structure [16] is shown in Table 1. The VCSEL is grown on a GaAs substrate. The bottom DBR consists of 40.5 pairs of AlGaAs while the top DBR has 23 pairs of AlGaAs. The active region is situated between the DBRs and contains three 7 nm GaAs quantum wells (QWs) separated by two 10 nm AlGaAs barrier layers. The oxide aperture is situated between the top DBR and the active zone.

The PC waveguide is assumed to be situated inside the VCSEL cavity between its DBRs as shown in Fig. 1 and created by air holes etched through spacer and active layers of the VCSEL. The PC defect is created by one missing hole. The diameter of PC holes a ranges from 0.1 to 5 μm and the ratio between the PC hole diameter d and the lattice constant a ranges from 0.1 to 0.9.

Assuming that the VCSEL operates with one longitudinal optical mode and m transverse modes, the electrical field in its resonator can be expressed as [17]

$$E(r, \theta, z, t) = \frac{1}{2} \sum_{j=1}^m \hat{e}_j E_j \phi_j(r, \theta) \exp(i(\beta_j z - \omega t)), \quad (1)$$

where j is the transverse mode index, \hat{e}_j is the polarization unit vector of the j -th mode, $\phi_j(r, \theta)$ is the j -th transverse mode distribution, β_j is the propagation constant of the j -th mode, $\omega = 2\pi/\lambda_0$ is the angular frequency of the optical mode and $\lambda_0 = 850$ nm is the vacuum wavelength. In PC fibre waveguides, the mode index $j=1$ corresponds to the fundamental LP₀₁ mode, $j=2$ and $j=3$ correspond to the two second-order LP₁₁ modes of the PC waveguide rotated 90° with respect to one another, $j=4$ and $j=5$ correspond to two LP₂₂ modes of the PC waveguide rotated 90° with respect to one another, $j=6$ corresponds to the LP₀₂ mode of the PC waveguide. However, the PC waveguide fabricated in an oxide-confined VCSEL is confined within the oxide aperture of the laser and thus modes of both the PC waveguide and the oxide confinement interplay. Some mode profiles of such PC-VCSEL are difficult to identify in terms of LP modes in that case and thus, for sake of simplicity, we associate the index j with mode order in the work. The fundamental mode of the PC-VCSEL has $j=1$ while high-order modes have indices exceeding one.

The transverse mode distribution $\phi_j(x, y)$ is computed by solving scalar Helmholtz equation with absorbing boundary condition [18]

$$\nabla_T^2 \phi_j(r, \theta) + \left(\left(n(r, \theta) \frac{\omega}{c_0} \right)^2 - \beta_j^2 \right) \phi_j(r, \theta) = 0, \quad (2)$$

where ∇_T^2 is the transverse Laplace operator, $n(r, \theta)$ is the transverse distribution of the refractive index in the PC-VCSEL waveguide, c_0 is the vacuum speed of light.

The eigenvalue problem (2) has been solved numerically for eigenvalues given by β_j using the Finite-Element Method of the Matlab Partial Differential Equation toolbox.

The transverse refractive index distribution in the oxide-confined PC-VCSEL is

$$n(r, \theta) = \begin{cases} n_a, r \leq r_a \\ n_a - \Delta n_{ox}, r > r_a, \\ 1, \text{ in holes} \end{cases} \quad (3)$$

where $n_a = 3.523$ is the mean refractive index [19], r_a is the radius of the oxide aperture, $\Delta n_{ox} = 6.567 \cdot 10^{-3}$ is the refractive index step introduced by the oxide [20] and computed as discussed in [19] for the VCSEL assuming the refractive index of the oxide material of 1.6.

Fig. 2 shows transverse optical mode distributions of the oxide-confined VCSEL normalized according to $(1/r_a^2) \int |\phi_j(r, \theta)|^2 r d\theta dr = 1$ [21]. Modes of the VCSEL are purely controlled by the oxide aperture as there is no other element providing the transverse variation of the refractive index in the VCSEL.

In this work, oxide-confined VCSELs with the PC of holes within the semiconductor VCSEL cavity are considered. The PC with the defect formed by one missing hole provides the waveguidance in the defect area. Thus, the PC around the defect operates as the waveguide cladding, and the defect in the PC provides the core for the waveguide. It is expected that the increasing the number of holes in the PC cladding in the transverse plane will introduce stronger control of waveguiding modes confined within the PC defect (up to some limit of hole number).

The PC introduced into the resonator of the oxide-confined VCSEL adds periodic transverse modulation of the refractive index and modifies the optical confinement. In that case, the competition between the transverse optical confinements made with the oxide aperture and the PC waveguide appears [8]. Thus, even if the oxide-confined VCSEL contains the single-

mode PC waveguide, the laser is not necessary single-mode as the oxide-confinement may establish multi-mode conditions. The strength of the oxide confinement depends on the refractive index step provided by the oxide Δn_{ox} which is influenced by the oxide layer thickness, its longitudinal position in the VCSEL resonator and the refractive index of the oxide [7,20,21]. Referring to waveguide theory of optical fibers, the number of waveguiding modes of a waveguide depends on the radius of the waveguide r_a and the refractive index step between the core and the cladding Δn_{ox} . Thus, the increase of Δn_{ox} results in the growth of the waveguiding mode number of the PC-VCSEL waveguide and may break single-mode conditions defined by the PC-waveguide.

Fig. 3 shows the transverse mode distributions of the oxide-confined PC-VCSELs computed for two values of Δn_{ox} . The characteristic shows that the transverse mode distribution of the high-order modes with $j=4$ and $j=5$ is influenced by the Δn_{ox} variation, while the fundamental mode distribution with $j=1$ is less influenced. The fundamental mode is less influenced by the Δn_{ox} variation because the mode is controlled mainly by the PC as it will be shown latter.

Transverse optical modes of the PC-VCSELs are analyzed in terms of their radii depicted in Fig. 3 and optical confinement factors both within the PC defect Γ_{pcj} and the oxide aperture

Γ_{oxj} defined as

$$\Gamma_{pcj} = \frac{\int_0^a \int_0^{2\pi} |\phi_j(r, \theta)|^2 r d\theta dr}{\int_0^\infty \int_0^{2\pi} |\phi_j(r, \theta)|^2 r d\theta dr}, \quad \Gamma_{oxj} = \frac{\int_0^{r_a} \int_0^{2\pi} |\phi_j(r, \theta)|^2 r d\theta dr}{\int_0^\infty \int_0^{2\pi} |\phi_j(r, \theta)|^2 r d\theta dr}. \quad (4)$$

The transverse optical confinement factors allow us to extract information about the modes of the PC-VCSEL waveguide, defining single- and multimode conditions of the waveguides. The value of the radii of the various modes allows us to estimate their output power assuming that their overlap with the uniform gain region scales with the area of overlap of the optical transverse mode and the carrier distribution within the gain region (which is taken as uniform neglecting any spatial hole burning). Thus the power should scale with r^2 of the transverse optical mode. To obtain more power in the fundamental mode its spatial extent in the transverse plane must be maximised. More precise theoretical estimation of power of the PC-VCSEL modes is possible with more complex models taking into account the interaction between photons and carriers in the PC-VCSEL [11,12].

Results and discussion

Single-mode conditions of PC waveguide

There are two transverse optical confinements in oxide-confined PC-VCSELs. Firstly, the confinement is provided by the oxide and the secondly it is given by the PC waveguide. Let us consider single-mode conditions of the PC waveguide assuming $\Delta n_{ox} = 0$ in (3) and thus, avoiding any effect of the oxide. Fig. 4 shows the difference between transverse optical confinement factors of the first and second transverse optical modes of the PC waveguide $\Gamma_{pc1} - \Gamma_{pc2}$ versus the lattice constant a and the ratio between the PC hole diameter and the lattice constant d/a . The stronger fundamental LP₀₁-like mode intensity confined within the PC defect is, the larger should be the confinement factor of the mode Γ_{pc1} . A waveguide mode confined within the PC waveguide core has the confinement factor Γ_{pcj} larger than zero. The confinement

factor of the weakly guided or non-guided mode approaches zero as virtually no field of the mode lies in the PC waveguide core. Thus, the single-mode operation appears if $\Gamma_{pc2} = 0$. If the second-order LP₁₁-like mode confined within PC defect appears, then $\Gamma_{pc2} > 0$ and $\Gamma_{pc1} - \Gamma_{pc2} < 1$. Thus, the distribution of $\Gamma_{pc1} - \Gamma_{pc2}$ defines single-mode conditions of the PC-waveguide and gives optimal PC configurations providing maximal confinement of the fundamental mode. The larger $\Gamma_{pc1} - \Gamma_{pc2}$ is, the stronger the confinement of single-fundamental mode. The single-fundamental-mode waveguidance appears at $d/a < 0.4$ if $a > 2 \mu\text{m}$. This conclusion is in agreement with previously published results for large a [22]. For smaller a the single-mode waveguidance at $d/a > 0.4$ is possible.

Effect of the PC geometry on transverse optical modes of the oxide-confined PC-VCSEL at fixed oxide confinement radius

In oxide-confined PC-VCSELs, the PC waveguide is incorporated within the VCSEL cavity and the competition between modes controlled by both the PC and the oxide appears. The effect of the oxide confinement is accounted in this part of the paper by assuming $\Delta n_{ox} = 6.567 \cdot 10^{-3}$ and $r_a = 8.5 \mu\text{m}$ in (3).

Fig. 5 shows the dependence of the confinement factors Γ_{pcj} on d/a and d for first five modes of the oxide-confined PC-VCSEL. According to Fig. 5a, as the d/a ratio grows, the confinement factor of the fundamental mode Γ_{pc1} increases. The confinement factor of the second-order mode is low for $d/a \leq 0.5$ and it is large for larger d/a ratio. The reason of this effect is that the second-order mode is guided and confined within the PC defect at $d/a > 0.5$ as

suggested by Fig. 4, while the mode is confined within the oxide aperture at $d/a \leq 0.5$. According to Fig. 5c, Γ_{pc4} is small at $d/a \leq 0.7$. Thus, the third-order mode is confined within the PC defect waveguide at $d/a > 0.7$. Otherwise, the mode is confined and controlled by the oxide aperture.

Let us now consider the effect of geometry of the PC on the radius of the electric field distribution of the fundamental mode shown in Fig. 6. The numerical method used for solving the eigenvalue problem represented by (2) has not converged at small values of a at $d/a < 0.3$. According to the Fig. 6, the larger a is, the larger radius of modal distribution r_1 is. The maximal radii of the mode appear at the smallest ratio of $d/a = 0.1$. The modeling results show that the radius of the fundamental mode of the VCSEL with no PC is $r_1 = 4.2966 \mu\text{m}$. Thus, the incorporation of the PC reduces the radius of the fundamental mode and thus is expected to lower the power of the PC-VCSEL fundamental mode.

Effect of the oxide confinement radius on transverse optical modes of the oxide-confined PC-VCSEL

Fig. 7 shows $\Gamma_{ox1} - \Gamma_{ox2}$ versus the lattice constant a and the oxide confinement radius r_a . The large value of $\Gamma_{ox1} - \Gamma_{ox2} > 0.5$ and the enhanced single-fundamental-mode are observed in the range of $r_a = 1 - 1.5 \mu\text{m}$. The maximal intensity of the single-fundamental mode is expected for the lattice constant $a = 0.5 \mu\text{m}$.

Fig. 8 shows $\Gamma_{ox1} - \Gamma_{ox2}$ versus r_a and d/a . The characteristic suggests that the smaller d/a ratio is, the larger $\Gamma_{ox1} - \Gamma_{ox2}$ is. In other words, small d/a ratio enhances the fundamental mode thanks to single-mode conditions given by the PC as displayed in Fig. 4.

Fig. 9 displays the transverse optical confinement factor of modes versus r_a for the VCSEL with no PC and PC-VCSELs with two PC geometries. According to the characteristic shown in Fig. 9a, higher-order modes of the VCSEL with no PC appear almost at any radius of the oxide aperture. The maximal difference between the confinement factors of the fundamental mode and the second-order mode appears at $r_a = 1\mu\text{m}$. Further increase of r_a results in the growth of the confinement factors of modes. Fig. 9b shows that the incorporation of a PC with $a = 0.5\mu\text{m}$ reduces the confinement factors of higher-order modes at $r_a < 5\mu\text{m}$ and increases the confinement factor of the fundamental mode. Confinement factors of all the modes reach their maxima at $r_a = 5\mu\text{m}$. Thus, the PC with a larger lattice constant of $a = 4\mu\text{m}$ has not allowed a significant reduction of the confinement factors of high-order modes compared to PC with smaller holes as seen in Fig. 9c. The dependence of the optical confinement factors of the PC-VCSEL is nearly same as for VCSELs with no PC. The effect of the PC can be observed for $r_a > a$ only and the confinement factors of high-order modes cannot be significantly reduced compared to VCSELs with no PC.

Table 2 shows values of the transverse confinement factors of first five modes of the VCSEL with no PC. It displays that the incorporation of the PC increases the transverse confinement factors. The improvement of the confinement factor is maximal with the PC made if small holes of $a = 0.5\mu\text{m}$ applied.

Minimal number of holes surrounding the PC defect

To compute the minimal hole number around the PC defect, let us consider the dependence of Γ_{ox1} on r_a shown in Fig. 10. The minimal radius of the oxide aperture r_a required to control the fundamental mode can be estimated from the characteristic as the minimal r_a allowing $\Gamma_{ox1} = 1$ (because $\Gamma_{ox1} = 1$ appears only if the PC controls the optical mode).

From the characteristic shown in Fig. 10 we can estimate the minimal r_a as $r_a = 2 \mu\text{m}$ at $a = 0.5 \mu\text{m}$, $r_a = 2.8 \mu\text{m}$ at $a = 1.0 \mu\text{m}$, $r_a = 3.8 \mu\text{m}$ at $a = 1.5 \mu\text{m}$ and $r_a = 4.9 \mu\text{m}$ at $a = 2.0 \mu\text{m}$. The dependence of a minimal r_a of the single-mode PC waveguide with $d/a = 0.4$ is shown in Fig. 11.

Thus, results shown in Fig. 11 suggest that at least 4 holes with the period a must be placed between the PC defect and the oxide aperture at $a = 0.5 \mu\text{m}$, 3 holes for $a = 1 - 4 \mu\text{m}$ and 2 holes for $a = 4 - 5 \mu\text{m}$. The results for $a = 1 - 4 \mu\text{m}$ are mostly in agreement with preliminary estimations for PC waveguides neglecting an oxide confinement published in [22].

Careful computations suggest that the minimal r_a depends on the d/a ratio. Fig. 12 shows the computed minimal r_a on d/a at $a = 4 \mu\text{m}$. According to the figure, the smaller d/a ratio is, the larger minimal r_a is. The choice of the PC with $a = 4 \mu\text{m}$ and $d/a = 0.4$ fabricated in the oxide-confined VCSEL with $r_a = 8.5 \mu\text{m}$ must allow sufficient control of the fundamental mode with the PC.

Conclusion

In this paper we have systematically investigated single-mode conditions of the PC waveguide: role of the oxide aperture size versus the a and d parameters of the PC, the number of periods of PC required, the confinement factors for the various transverse modes and their physical size.

We have identified that there are competing optimization issues between power and transverse mode discrimination. We have demonstrated that the single mode waveguidance is possible for $d/a > 0.4$ at $a < 2 \mu\text{m}$. The incorporation of the PC waveguide into oxide-confined VCSELs leads to the competition between optical modes controlled by both transverse waveguides of the PC and the oxide aperture.

The oxide confinement radius r_a was found to be a significant factor influencing the transverse mode control of the VCSELs and PC-VCSELs. Single-mode guidance appears at small oxide radii of oxide-confined VCSEL with no PC. The PC fabricated in the VCSEL allows the control of the optical mode confined within its defect at $r_a > a$, and its effect is stronger for smaller a . For instance, high-order modes of PC-VCSEL with $a = 0.5 \mu\text{m}$ $d/a = 0.4$ and $r_a < 5 \mu\text{m}$ have much smaller confinement factors within the oxide aperture compared to VCSELs with no PC. However, the effect of the PC almost disappears for the PC with increased lattice constant of $a = 4 \mu\text{m}$.

It was shown that the lattice constant a defines the radius of the fundamental mode and therefore its power – the larger a is, the larger power of the mode is. However, a cannot be increased infinitely because the PC index confinement gets weaker at $a > r_a / 2.5$ ($d/a = 0.4$) and completely disappears at $a > r_a$. It would be expected that to increase the power of single-mode radiation, the radius of the oxide confinement r_a can be increased. However, our results have shown that the confinement radius r_a can be increased up to 3-4 μm keeping the PC-VCSEL single-mode. High-order modes confined within oxide emerge if a further increase of the confinement radius appears. The PC waveguide is found to be unable to control these modes

confined within the oxide because the refractive index step provided by the oxide is normally larger than the step provided by the PC.

It was shown that the fundamental mode of the PC-VCSEL controlled with the PC has smaller radius compared to the fundamental mode of the VCSEL with no PC. Therefore, the power of the fundamental mode of the PC-VCSEL can be expected to be smaller than the power of the mode of VCSEL with no PC.

Results show that there are two possible scenarios in enhancing the fundamental mode with the PC in PC-VCSELS. Firstly, the single-mode PC waveguide can be fabricated in oxide-confined VCSELS with the wide oxide confinement of $r_a > 5 \mu\text{m}$. Geometrical parameters of the PC must be selected according to characteristic shown in Fig. 4 of the paper satisfying the condition $a \leq r_a/2.5$. In that case, the PC allows maximal power of the fundamental mode but relatively low high-order mode suppression can be expected. Secondly, the single-mode PC waveguide can be fabricated in oxide-confined VCSELS with the narrow oxide confinement of $r_a < 5 \mu\text{m}$. Smaller hole diameter must be chosen to satisfy the condition $a \leq r_a/2.5$. In that case, both narrow oxide aperture and the PC waveguide enhance the fundamental mode of the PC-VCSEL by reducing the transverse confinement factors of high-order modes. However, such a configuration of the PC-VCSEL is expected to result in lower power for the fundamental mode because of the small radius of the mode and small overlap between the area of the mode and active zone of the VCSEL.

References

- [1] Vertical-cavity surface-emitting laser devices, H. Li and K. Iga (Eds.), Springer, 2003.

- [2] W.D. Zhou, J. Sabarinathan, B. Kochman, E. Berg, O. Qasaimeh, S. Pang, and P. Bhattacharya, “Electrically injected single-defect photonic bandgap surface-emitting laser at room temperature,” *Electron. Lett.*, **36**, 1541–1542 (2000).
- [3] H. Unold, M. Golling, R. Michalzik, D. Supper, and K. Ebeling, “Photonic crystal surface-emitting lasers: tailoring waveguiding for single-mode emission,” in *Proc. European Conference on Optical Communication, ECOC 2001, Amsterdam, Netherlands*, 520–521 (2001).
- [4] Dae-Sung Song, Se-Heon Kim, Hong-Guy Park, Chang-Kyu Kim, and Yong-Hee Lee, “Single-fundamental-mode photonic-crystal vertical-cavity surface-emitting lasers,” *Appl. Phys. Lett.*, **80**, 3901–3903 (2002).
- [5] N. Yokouchi, A.J. Danner, and K.D. Choquette, “Two-dimensional photonic crystal confined vertical-cavity surface-emitting lasers,” *IEEE J. of Selected Topics in Quant. Electron*, **9**, 1439–1445 (2003).
- [6] T.A. Birks, J.C. Knight, and P.St.J. Russell, “Endlessly single-mode photonic crystal fiber,” *Opt Lett.*, **22**, 961–963 (1997).
- [7] P.S. Ivanov, M. Dragas, M. Cryan, and J.M. Rorison, “Theoretical investigation of transverse optical modes in photonic-crystal waveguides imbedded into proton-implanted and oxide-confined vertical-cavity surface-emitting lasers,” *J. Opt. Soc. Am. B*, **22**, 2270–2276 (2005).
- [8] T. Czynszanowski, M. Dems, and K. Panajotov, “Single mode condition and modes discrimination in photonic-crystal 1.3 μm AlInGaAs/InP VCSEL,” *Optics Express*, **15**, pp.5604-5609 (2007).
- [9] D.F. Siriani, Meng Peun Tan, A.M. Kasten, A.C.L. Harren, P.O. Leisher, J.D. Sulkin, J.J. Raftery, A.J. Danner, A.V. Giannopoulos, K.D. Choquette, “Mode Control in Photonic Crystal

Vertical-Cavity Surface-Emitting Lasers and Coherent Arrays,” IEEE Journal of Selected Topics in Quantum Electronics, **15**, pp. 909-917 (2009).

[10] P. Ivanov, M. Cryan, and J. Rorison, “PC-VCSELs: Comparisson of Modelling and Experimental Results,” in Proc. A Future in Light: International Conference on Photonics, Metz, France, p. 10 (2009).

[11] P. Ivanov, Y. Zhu, M. Cryan, and J. Rorison, “Theoretical investigation of characteristics of vertical-cavity surface-emitting lasers incorporating two-dimensional photonic crystals,” in Proc. COST 288 meeting, Metz, France (2007). Slides available online from COST 288 website: <http://www.een.bris.ac.uk/cost288/metz07ppt/ivanov.ppt>

[12] P. Nyakas, T. Kise, T. Karpati, and N. Yokouchi, “Numerical optimization of single-mode photonic crystal VCSELs”, in Proc. NUSOD, Nottingham, United Kingdom, 93–94 (2008).

[13] P.S. Ivanov, M. Cryan, P. Heard, and J. Rorison, “Vertical-Cavity Lasers with Photonic Crystals,” in Proc. Photonex, Coventry, United Kingdom (2009).

[14] H. Matsubara, S. Yoshimoto, H. Saito, Y. Jianglin, Y. Tanaka, and S. Noda, “GaN Photonic-crystal surface-emitting laser at blue-violet wavelengths,” Science, **319**, 445-447 (2008).

[15] M. Dems, R. Kotynski, and K. Panajotov, “Plane wave admittance method – a novel approach for determining the electromagnetic modes in photonic structures,” Optics express, **13**, 3196-3207 (2005).

[16] C.C. Choi, Thin-film VCSELs and optical interconnection layer fabrications for fully embedded board level optical interconnects, PhD thesis, The University of Texas at Austin, 2003, Available online <http://repositories.tdl.org/tdl/handle/2152/173>

- [17] J.Y. Law and G.P. Agrawal, "Effects of spatial hole burning on gain switching in vertical-cavity surface-emitting lasers," *IEEE J. Quantum Electron.* **33**, 462–468 (1997).
- [18] J. Shibayama, T. Takahashi, J. Yamauchi, and H. Nakano, "Comparative study of absorbing boundary conditions for the time-domain beam propagation method," *IEEE Photon. Technol. Lett.* **13**, 314–316 (2001).
- [19] R. Michalzik, "Simple understanding of waveguiding in oxidized VCSELs," Annual Report of Optoelectronics Department of University of Ulm, 1995, pp. 19-23, available online: <http://www-opto.e-technik.uni-ulm.de/>
- [20] G.R. Hadley, "Effective index model for vertical-cavity surface-emitting lasers," *Optics Lett.*, **20**, 1483–1485 (1995).
- [21] S. Riyopoulos and D. Dialetis, "Ultrafast Simulations of Multimode VCSEL Using Optimized Waist Paraxial Eigenmodes," *IEEE Journal of Selected Topics in Quantum Electronics*, **9**, 892–904 (2003).
- [22] P.S. Ivanov, H.J. Unold, R. Michalzik, J. Maehns, K.J. Ebeling, and I.A. Sukhoivanov, "Theoretical study of cold-cavity single-mode conditions in vertical-cavity surface-emitting lasers with incorporated two-dimensional photonic crystals," *JOSA B*, **20**, 2442–2447 (2003).

Fig. 1. Schematic figure of the PC-VCSEL cavity.

Fig. 2. Normalized transverse distributions of first five modes and their relative radii r_j taken at half-maximum.

Fig. 3. Normalized transverse distributions of first five modes of the oxide-confined PC-VCSEL with $a = 4 \mu\text{m}$, $d = 0.4a$, and $r_a = 5 \mu\text{m}$. (a) $\Delta n_{ox} = 6.567 \cdot 10^{-3}$ and (b) $\Delta n_{ox} = 2.2508$.

Fig. 4. $\Gamma_{pc1} - \Gamma_{pc2}$ for first LP₀₁-like mode ($j=1$) and second LP₁₁-like mode ($j=2$) of the PC-waveguide versus a and d/a .

Fig. 5. Confinement factors of modes confined within the PC defect Γ_{pcj} versus a and d/a (a) $j=1$, (b) $j=2$ and (c) $j=4$. $r_a = 8.5 \mu\text{m}$.

Fig. 6. Radii of fundamental mode distributions taken at half-maximum versus a and d/a for $r_a = 8.5 \mu\text{m}$.

Fig. 7. The $(\Gamma_{ox1} - \Gamma_{ox2})$ plotted against a and r_a for $d/a = 0.4$.

Fig. 8. The $(\Gamma_{ox1} - \Gamma_{ox2})$ plotted against d/a and r_a for $a = 4 \mu\text{m}$.

Fig. 9. Γ_{oxj} plotted against mode index j and r_a . (a) VCSEL with no PC, (b) PC-VCSEL with $a = 0.5 \mu\text{m}$ for $d/a = 0.4$ and (c) PC-VCSEL with $a = 4 \mu\text{m}$ for $d/a = 0.4$.

Fig. 10. The dependence of Γ_{ox1} on r_a and a for $d/a = 0.4$.

Fig. 11. The minimal r_a required to control the fundamental mode versus a for $d/a = 0.4$.

Fig. 12. The minimal r_a required to control the fundamental mode versus d/a for $a = 4 \mu\text{m}$.

Table 1. Epitaxial VCSEL structure.

Material	x	Thickness, nm	Refractive index	Description
GaAs		5	3.675	
$\text{Al}_x\text{Ga}_{(1-x)}\text{As}$	0.16	5	3.505	
$\text{Al}_x\text{Ga}_{(1-x)}\text{As}$	0.16	41.1	3.505	Top DBR 23 repetitions
$\text{Al}_x\text{Ga}_{(1-x)}\text{As}$	0.92->0.16	20	3.031->3.505	
$\text{Al}_x\text{Ga}_{(1-x)}\text{As}$	0.92	49.3	3.031	
$\text{Al}_x\text{Ga}_{(1-x)}\text{As}$	0.16->0.92	20	3.505->3.031	
$\text{Al}_x\text{Ga}_{(1-x)}\text{As}$	0.16	19.5	3.505	
$\text{Al}_x\text{Ga}_{(1-x)}\text{As}$	0.98->0.16	20	3.00->3.505	
$\text{Al}_x\text{Ga}_{(1-x)}\text{As}$	0.98	30	3.00	Oxide layer
$\text{Al}_x\text{Ga}_{(1-x)}\text{As}$	0.92	55.1	3.031	
$\text{Al}_x\text{Ga}_{(1-x)}\text{As}$	0.6	95.3	3.122	
$\text{Al}_x\text{Ga}_{(1-x)}\text{As}$	0.3	11	3.401	
GaAs		7	3.675	QW
$\text{Al}_x\text{Ga}_{(1-x)}\text{As}$	0.3	10	3.401	
GaAs		7	3.675	QW
$\text{Al}_x\text{Ga}_{(1-x)}\text{As}$	0.3	10	3.401	
GaAs		7	3.675	QW
$\text{Al}_x\text{Ga}_{(1-x)}\text{As}$	0.3	11	3.401	
$\text{Al}_x\text{Ga}_{(1-x)}\text{As}$	0.6	95.3	3.122	
$\text{Al}_x\text{Ga}_{(1-x)}\text{As}$	0.92	59.6	3.031	
$\text{Al}_x\text{Ga}_{(1-x)}\text{As}$	0.16->0.92	20	3.505->3.031	
$\text{Al}_x\text{Ga}_{(1-x)}\text{As}$	0.16	41.1	3.505	Bottom DBR: 40 repetitions
$\text{Al}_x\text{Ga}_{(1-x)}\text{As}$	0.92->0.16	20	3.031->3.505	
$\text{Al}_x\text{Ga}_{(1-x)}\text{As}$	0.92	49.3	3.031	
$\text{Al}_x\text{Ga}_{(1-x)}\text{As}$	0.16->0.92	20	3.505->3.031	
$\text{Al}_x\text{Ga}_{(1-x)}\text{As}$	0.16	10	3.505	
GaAs		500	3.53	
$\text{Al}_x\text{Ga}_{(1-x)}\text{As}$	0.98	100	3.00	
GaAs			3.675	Substrate

Table 2. Transverse confinement factor of the VCSELs and PC-VCSELs with $r_a = 8.5 \mu\text{m}$.

j	No PC	PC, $a = 4 \mu\text{m}$, $d/a = 0.4$	PC, $a = 0.5 \mu\text{m}$, $d/a = 0.4$
1	0.9982	0.9999	1.0000
2,3	0.9953	0.9992	1.0000
4,5	0.9914	0.9959	1.0000

Published by

OSA

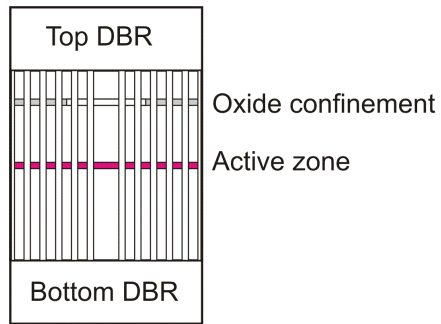


Fig. 1. Schematic figure of the PC-VCSEL cavity.

Published by
OSSA

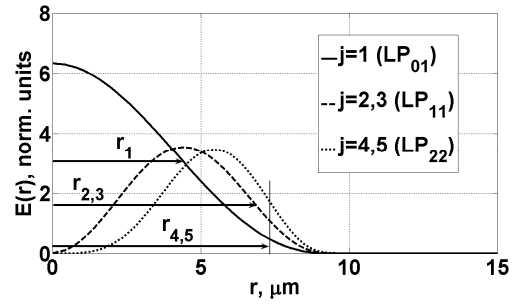
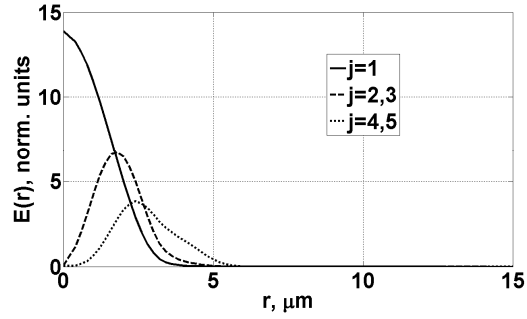


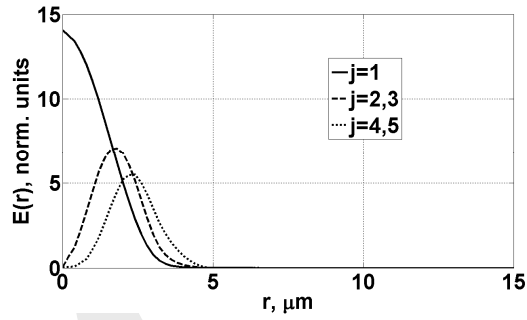
Fig. 2. Normalized transverse distributions of first five modes and their relative radii r_j taken at half-maximum.

Published by

OSA



a)



b)

Fig. 3. Normalized transverse distributions of first five modes of the oxide-confined PC-VCSEL with $a = 4 \mu\text{m}$, $d = 0.4a$, and $r_a = 5 \mu\text{m}$. (a) $\Delta n_{ox} = 6.567 \cdot 10^{-3}$ and (b) $\Delta n_{ox} = 2.2508$.

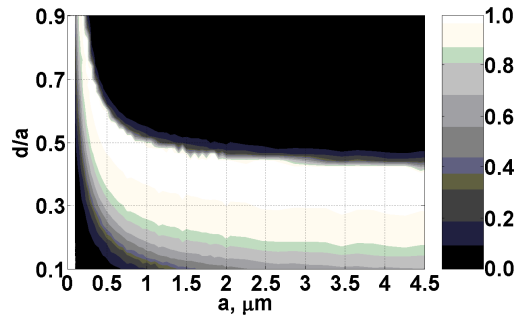
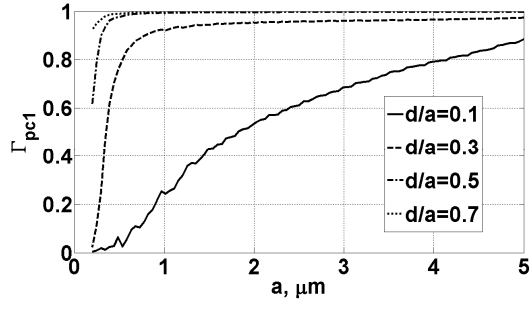


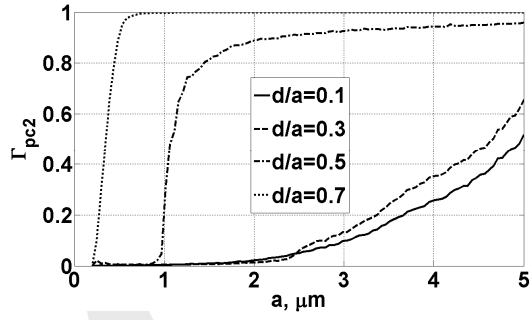
Fig. 4. $\Gamma_{pc1} - \Gamma_{pc2}$ for first LP_{01} -like mode ($j=1$) and second LP_{11} -like mode ($j=2$) of the PC-waveguide versus a and d/a .

Published by

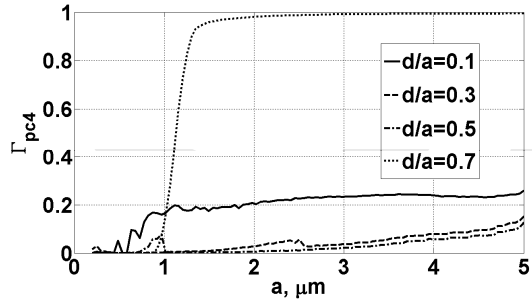
OSA



a)



b)



c)

Fig. 5. Confinement factors of modes confined within the PC defect Γ_{pcj} versus a and d/a (a)

$j=1$, (b) $j=2$ and (c) $j=4$. $r_a=8.5 \mu\text{m}$.

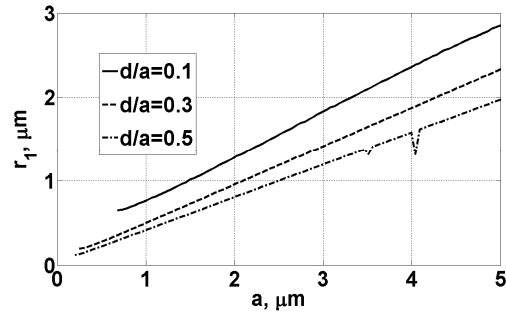


Fig. 6. Radii of fundamental mode distributions taken at half-maximum versus a and d/a for

$r_a = 8.5 \mu\text{m}$.

Published by

OSA

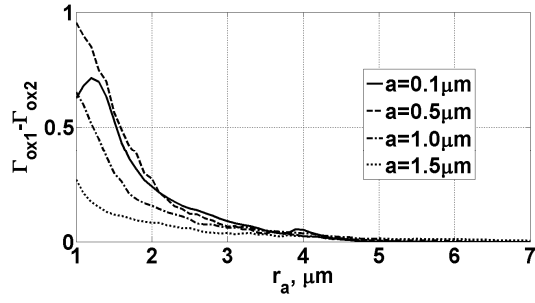


Fig. 7. The $(\Gamma_{ox1} - \Gamma_{ox2})$ plotted against a and r_a for $d/a = 0.4$.

Published by

OSA

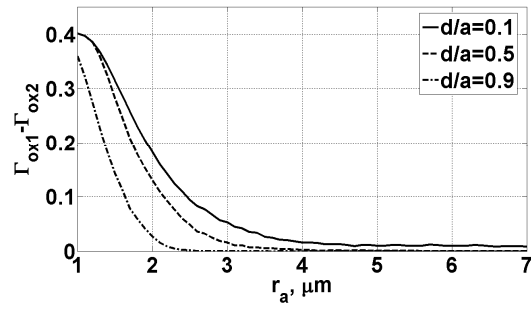
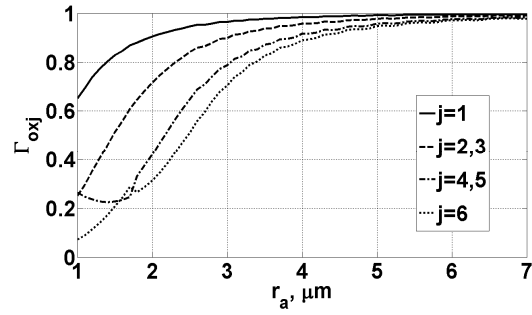


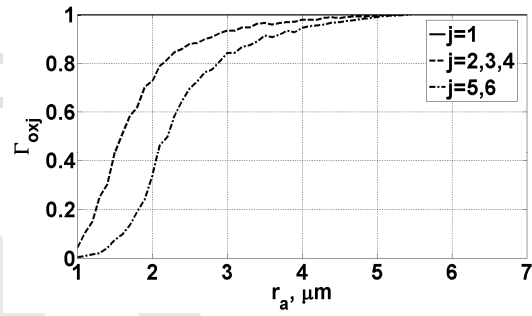
Fig. 8. The $(\Gamma_{ox1} - \Gamma_{ox2})$ plotted against d/a and r_a for $a = 4 \mu\text{m}$.

Published by

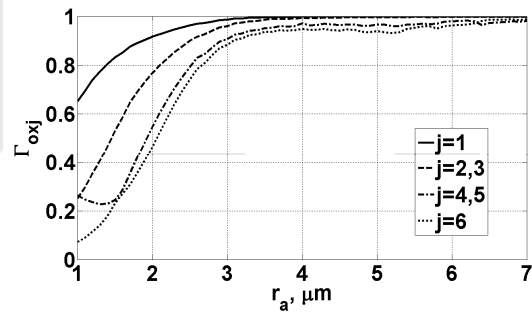
OSA



a)



b)



c)

Fig. 9. Γ_{oxj} plotted against mode index j and r_a . (a) VCSEL with no PC, (b) PC-VCSEL with $a = 0.5 \mu\text{m}$ for $d/a = 0.4$ and (c) PC-VCSEL with $a = 4 \mu\text{m}$ for $d/a = 0.4$.

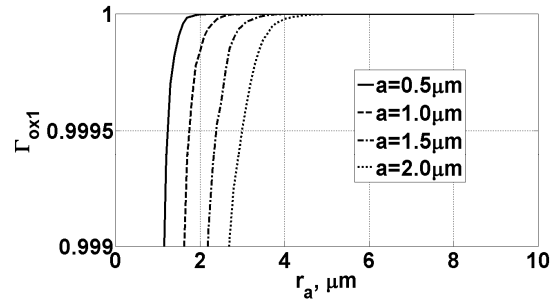


Fig. 10. The dependence of Γ_{ox1} on r_a and a for $d/a=0.4$.

Published by

OSSA

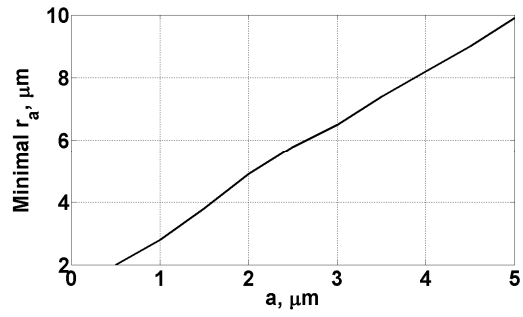


Fig. 11. The minimal r_a required to control the fundamental mode versus a for $d/a = 0.4$.

Published by

OSA

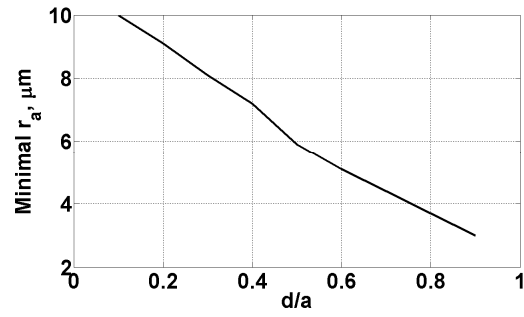


Fig. 12. The minimal r_a required to control the fundamental mode versus d/a for $a = 4 \mu\text{m}$.

Published by
OSSA